



Analysis of Ventilation Architectures for Data Center Cooling Using Steady and Transient Computational Fluid Dynamics Simulations



Leila Riahinezhad¹ , Melika Mohammadkhah² , Ahmad Nooraeen^{3*} 

¹ Department of Sustainability and Energy, Mammut Group Company, 1513737511 Tehran, Iran

² Institute of Mechanics, Technische Universität Berlin, 10623 Berlin, Germany

³ Faculty of Biomedical Engineering, Amirkabir University of Technology, 1149754413 Tehran, Iran

* Correspondence: Ahmad Nooraeen (ahmad.nooraeen@gmail.com)

Received: 08-14-2025

Revised: 09-13-2025

Accepted: 09-22-2025

Citation: L. Riahinezhad, M. Mohammadkhah, and A. Nooraeen, "Analysis of ventilation architectures for data center cooling using steady and transient computational fluid dynamics simulations," *Math. Model. Sustain. Eng.*, vol. 1, no. 1, pp. 48–62, 2025. <https://doi.org/10.56578/mmse010104>.



© 2025 by the author(s). Licensee Acadlore Publishing Services Limited, Hong Kong. This article can be downloaded for free, and reused and quoted with a citation of the original published version, under the CC BY 4.0 license.

Abstract: Efficient management of airflow and heat dissipation in data centers is becoming increasingly critical as computing densities increase and thermal loads grow. To address these challenges, this study numerically examines the thermo-fluid behavior of a medium-sized data center containing twelve heat-generating server racks under multiple ventilation strategies. A three-dimensional CFD model was developed using the RANS equations with the SST $k-\omega$ turbulence formulation and the Boussinesq approximation to account for buoyancy-driven flow. Eight ventilated configurations were evaluated by combining two louver orientations (20° and 50°), two inlet heights (top or bottom), and two inlet velocity modes (constant or pulsatile), in addition to a no-ventilation control scenario. Both steady and transient simulations were performed to capture the interactions between inlet momentum, recirculation patterns, and thermal stratification over a one-hour operational period. The control case exhibited strong thermal stratification and a stable hot layer beneath the ceiling, demonstrating the inadequacy of natural convection alone. Introducing ventilation significantly modified the airflow topology and improved cooling performance, though with considerable sensitivity to inlet design. Shallower-angle louvers (20°) enhanced horizontal jet penetration and reduced recirculation pockets, whereas steeper louvers (50°) generated stronger impingement and more localized hot spots. Inlet height further shaped vertical temperature distribution: bottom inlets effectively cooled lower and mid-rack levels, while top inlets reduced ceiling-layer temperatures by disrupting buoyant plumes. Pulsatile ventilation outperformed constant inflow by periodically increasing momentum, enhancing mixing, and weakening plume formation during peak phases. Mass-flow analysis similarly showed that extraction capacity strongly correlated with inlet velocity amplitude. Overall, the results highlight the importance of coordinated selection of inlet position, louver angle, and temporal forcing. The combined use of shallow-angle louvers and pulsatile ventilation presents a promising pathway for improving cooling uniformity and thermal management in high-density data centers.

Keywords: Data center cooling; Buoyancy-driven airflow; Louver ventilation; Pulsatile inlet flow; CFD thermal analysis

1 Introduction

The rapid expansion of high-performance computing and cloud services has led to a significant increase in power density within modern data centers (DCs) [1]. This concentrated power consumption generates intense thermal loads, making heat removal the most critical determinant of DC operation, reliability, and cost [2]. Ineffective thermal management results in elevated component temperatures, thermal throttling, and localized hotspots, ultimately reducing server lifespan and system stability [3]. Moreover, cooling systems, including fans and chillers, consume 30% to 50% of the total operational energy budget, underscoring the importance of optimizing heat transfer to achieve low Power Usage Effectiveness (PUE) [4, 5].

Given the complex thermo-fluid phenomena involved, turbulent airflow, buoyancy-driven plumes, and conduction through densely packed equipment, accurate thermal analysis requires advanced methodologies [6]. Experimental testing alone is costly, intrusive, and incapable of exploring the vast design space associated with different layouts and operating conditions [7]. Consequently, Computational Fluid Dynamics (CFD) has emerged as the primary tool for

mapping the thermal field and evaluating convective heat transfer from heated server components (modeled here as solid aluminum volumes) [8, 9]. CFD enables visualization of crucial processes such as thermal stratification and air short-circuiting, making it indispensable for identifying geometric and operational variables that influence cooling performance [10].

Early DC studies relied heavily on steady-state CFD because it provides equilibrium temperature and velocity fields under fixed operating conditions [11]. While useful for identifying baseline design issues, steady-state analysis cannot capture the dynamic behavior inherent to modern IT environments, where workloads fluctuate and thermal loads vary rapidly [12]. It also fails to predict thermal resilience during transient events such as cooling system failures or phased equipment startup [13]. Transient CFD resolves these limitations by modeling the evolution of the thermal field over time with time-varying heat loads and boundary conditions [14]. This capability is essential for assessing parameters such as thermal ride-through time during cooling outages [15] and for supporting modern control strategies, including model predictive control and reinforcement learning, whose optimization algorithms depend on accurate transient data [16]. Thus, transient CFD is a prerequisite for designing resilient, energy-optimal next-generation DCs [17].

Introducing a pulsatile flow regime into the cooling system offers a promising pathway for reducing electrical energy consumption [18]. Periodic oscillation disrupts the thermal boundary layer and enhances mixing, increasing convective heat transfer effectiveness compared to steady flow [18]. This improvement enables the same heat removal to be achieved with a lower mean volumetric flow rate [19]. Because fan power follows a cube-law relationship with flow rate, even modest reductions in average airflow translate into substantial energy savings, potentially lowering the facility's PUE when the energy cost of pulsation is favorable [19].

The comparative analysis of Up (Ceiling) and Bottom (Raised Floor) inlet strategies addresses a central question in DC ventilation design. Raised-floor systems, historically common, use a pressurized plenum to deliver cold air but are prone to bypass flow and performance degradation due to cable congestion [20]. Ceiling-based (Up) inlet systems, increasingly preferred in high-density environments, rely on high-momentum diffusers to direct cool air toward the cold aisle [21]. Diffusers with larger deflection angles enhance the Coanda effect, allowing supply air to adhere to the ceiling, increase its throw distance, and promote more uniform cooling across the room width before descending into the server aisles [22, 23]. Proper optimization of the louver angle minimizes short-circuiting and recirculation of hot air back into the inlets [24].

The lack of a comprehensive, high-fidelity transient CFD investigation that simultaneously evaluates the combined influence of an active heat transfer enhancement technique, such as pulsatile flow, and critical geometric control parameters like Inlet Position and Louver Angle, represents a significant gap in the literature on DC thermal management. The primary goal of this study is to directly address factors influencing efficient heat removal, a process fundamental to maximizing DC reliability and minimizing operational cost. To achieve this, the present research executes nine distinct, transient and steady-state CFD simulations to provide a holistic understanding of their coupled effects on thermal performance. Specifically, the study first aims to quantify the thermal-hydraulic performance by accurately mapping the air velocity field and the spatial temperature distribution to precisely identify localized hotspots and thermal stratification. Crucially, it seeks to determine the potential of the pulsatile flow regime to significantly enhance heat transfer effectiveness and reduce the time-averaged temperatures recorded at the server inlets, thereby maximizing cooling capacity. Finally, the investigation will identify the optimal combination of inlet position and louver angle that maximizes cooling efficiency and minimizes the required mass flow rate at the outlet, ultimately delivering robust, evidence-based guidelines for the design and dynamic control of cooling systems in next-generation high-density DCs.

2 Methods and Materials

This study employs a three-dimensional CFD framework to investigate thermo-fluid behavior in a data-center environment equipped with heat-generating racks and multiple ventilation configurations. The computational methodology integrates detailed geometric modeling, boundary-condition specification, turbulence and energy-equation formulations, and mesh-independence verification to ensure accurate prediction of buoyancy-affected airflow and thermal fields.

2.1 Geometry

Figure 1 presents the detailed geometric configuration of the data center used in numerical simulations. The computational domain was constructed as a fully enclosed rectangular room with overall dimensions of 8 m in length, 7 m in width, and 3 m in height, representing the typical architectural proportions of a medium-scale server facility. This enclosure provides sufficient volume for the development of thermal plumes, buoyancy-driven recirculation regions, and ventilation jet interactions, ensuring that the simulated environment reflects realistic airflow behavior found in practical data centers.

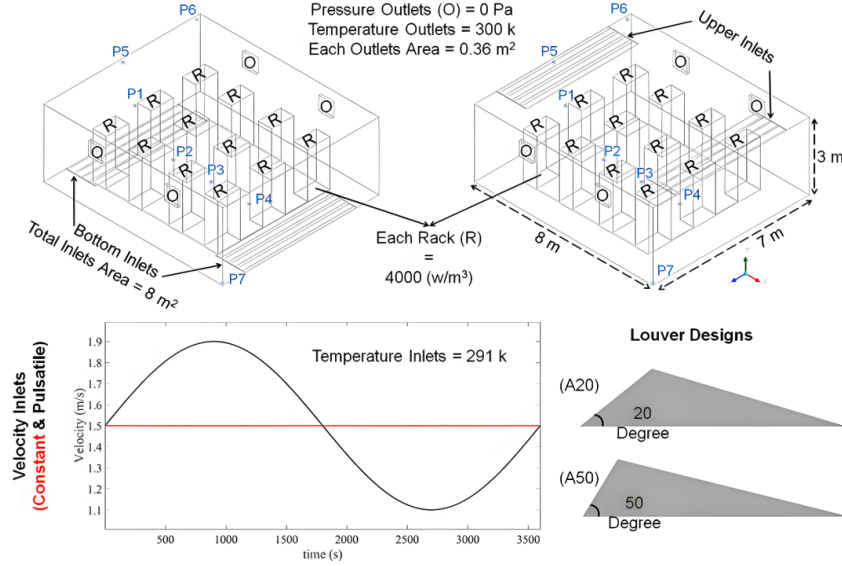


Figure 1. 3D data center model showing ventilation layout and monitoring points

Within this room, twelve server racks were arranged in a systematic layout to mimic standard equipment organization. Each rack was modeled as a rectangular solid block, positioned vertically on the floor and extending upward to a height representative of full-size server cabinets. To accurately capture thermal conduction and internal heat distribution, the racks were defined as solid aluminum volumes, allowing the model to represent the spreading of heat through the rack structure before transferring it to the surrounding air.

The placement of the racks within the domain was designed to create alternating corridors consistent with conventional data center arrangements. This spatial organization introduces natural airflow channels between rows, enabling the formation of rising hot air plumes above each rack and lateral mixing in the upper regions of the room. The distances between racks and between racks and the surrounding walls were selected to prevent blockage of airflow pathways while still maintaining realistic equipment density.

In addition to the rack geometry, the room includes designated regions for louvers (air inlets) and outlet vents, which are integral components of the geometric domain. The louvers were incorporated as planar surfaces embedded into either the upper or lower section of the room's side walls, depending on the scenario. Their orientation could be adjusted to either 20° or 50°, and these angular configurations were explicitly included in the geometric model to capture the directional characteristics of the incoming ventilation jets. Similarly, four outlet vents were positioned on the walls as discrete openings, allowing the domain to accommodate realistic air extraction paths without altering the primary room geometry.

2.2 CFD Simulation: Governing Equations and Turbulence Modeling

Airflow and heat transfer within the data center were simulated using ANSYS Fluent 16.1. The numerical model solves the coupled conservation equations of mass, momentum, and energy to capture the transient thermo-fluid behavior induced by buoyancy forces, forced ventilation, and heat generation from the server racks. Air was treated as an incompressible Newtonian fluid, and density variations were incorporated using the Boussinesq approximation [25]. The air properties are provided in Table 1. This approach allows efficient computation while accurately representing thermally driven flow motion inside the room.

The governing flow field was computed using the Reynolds-Averaged Navier-Stokes (RANS) formulation. Turbulence effects were represented through the Shear Stress Transport (SST) $k-\omega$ model, which blends the robustness of the standard $k-\omega$ model in near-wall regions with the predictive capability of the $k-\omega$ model in free-shear zones. Given the presence of strong recirculation zones, jet-like inflow structures from the louvers, and buoyancy-induced plumes rising above the server racks, the SST $k-\omega$ model provides superior fidelity in predicting flow separation, streamline curvature, and heat-transfer behavior throughout the data center [26]. The governing equations solved in the domain are presented below.

$$\frac{\partial (\rho u_i)}{\partial x_i} = 0 \quad (1)$$

where, ρ denotes the fluid density, u_i is the velocity component.

$$\frac{\partial(\rho u_i u_j)}{\partial x_j} = -\frac{\partial P}{\partial x_i} + \frac{\partial}{\partial x_j} \left[\mu \left(\frac{\partial u_i}{\partial x_j} + \frac{\partial u_j}{\partial x_i} \right) \right] + \frac{\partial \tau_{ij}}{\partial x_j} + \rho g_i \quad (2)$$

where, P represents the static pressure, and μ is the dynamic viscosity of the fluid. The term τ_{ij} corresponds to the Reynolds stress tensor, while g_i indicates the body force component.

$$\frac{\partial(\rho u_i h)}{\partial x_j} = \frac{\partial}{\partial x_j} \left[k_{eff} \frac{\partial T}{\partial x_j} \right] + S_h + \rho u_j g_i \quad (3)$$

The symbol h refers to the specific enthalpy, k_{eff} is the effective thermal conductivity accounting for both molecular and turbulent contributions, and S_h represents the volumetric source term associated with heat generation within the domain.

Table 1. List of the constants used for the CFD simulation [27]

Constant	Value (Unit)
Fluid density	1.184 (kg/m ³)
Specific heat	1005 (J/kg·K)
Thermal conductivity	0.025 (W/m·K)
Viscosity	1.81×10 ⁻⁵ (kg/m·s)

2.3 Boundary Conditions

The boundary conditions applied to the computational domain were defined to replicate realistic thermal and ventilation conditions within the data center. Two different inflow conditions were prescribed at the louvers [28]. In the first group of simulations, a constant uniform inlet velocity of 1.5 m/s was specified. In the second group, a pulsatile velocity profile was imposed, defined by a sinusoidal waveform with a mean velocity of 1.5 m/s and an amplitude of 0.4 m/s, resulting in instantaneous inlet velocities oscillating between 1.1 m/s and 1.9 m/s throughout the simulation. In all cases, the incoming air was assigned a constant temperature of 291 K, representing cooled supply air delivered by a specific unit.

Air was discharged from the data center through four outlet vents distributed along the room's side walls. These outlets were implemented using a zero pressure boundary condition (0 Pa gauge) to allow natural extraction driven by internal pressure fields and buoyancy effects. The placement and size of the outlets remained identical for all simulation scenarios, ensuring consistent ventilation capacity across the parametric study. To assess the impact of ventilation absence, one additional configuration, referred to as the Control case, was evaluated with all inlet boundaries disabled, leaving only the passive outlets active. This scenario allowed investigation of the thermal rise in a fully sealed room without forced cooling.

Internal heat generation was modeled by applying a uniform volumetric heat flux of 4000 W/m³ to each of the twelve aluminum server racks [29]. The heat flux value represents a moderate operational thermal load consistent with contemporary high-density server systems. To account for thermal interaction with the environment, all room walls, floor, and ceiling were treated as isothermal boundaries held at 303 K, representing the thermal influence of the building envelope and preventing artificial heat accumulation at the enclosure boundaries.

Gravity was activated in the y -direction, enabling buoyancy-driven flow behavior arising from temperature gradients within the room. The simulations were categorized into steady-state and transient groups depending on the inlet condition. Cases with constant inflow velocity were solved under steady-state assumptions, while scenarios with pulsatile inlet excitation were performed as fully transient simulations over a physical duration of one hour, allowing the model to resolve time-dependent thermal oscillations and dynamic airflow development. The summary of boundary conditions is provided in Table 2.

The resulting set of nine computational scenarios, summarized in Table 3, covers all combinations of inlet type, inlet position, and louver angle, including the control case with no ventilation. This configuration establishes a comprehensive basis for studying airflow patterns and transient temperature fluctuations within the data center.

A mesh independence study was conducted to ensure that the numerical results were not affected by grid resolution. Three mesh sizes, coarse, medium, fine, and finer were tested, corresponding to approximately 400 mm, 200 mm, 100 mm, and 50 mm respectively. For each mesh, the mass flow rate at the exhaust outlets was used as the primary convergence metric because it directly reflects the global flow distribution inside the data-center enclosure.

Mesh independence was considered achieved when the variation in outlet mass flow rate between two consecutively refined meshes dropped below 2%. The results showed a 1.4% difference between the fine and finer meshes, confirming mesh independence.

Table 2. Summary of boundary conditions used in the CFD model

Boundary / Region	Applied Condition	Value	Source
Fresh-air inlet (louver)	Velocity inlet	Constant: 1.5 m/s Pulsatile: 1.1–1.9 m/s	[30]
Fresh-air inlet (louver)	Temperature	291 °K	[31]
	Turbulence intensity (%)	5%	[32]
Rack heat load (volumetric)	Heat generation rate	4000 W/m ³	[29]
Exhaust outlets above racks	Pressure outlet	0 Pa	[33]

Table 3. Nine simulation cases covering all inlet configurations, plus control case

No.	Inlet	Position of Inlet	Luover Angle (Degree)
0	Control	—	—
1	Constant	up	20
2	Constant	up	50
3	Constant	bottom	20
4	Constant	bottom	50
5	Pulsatile	up	20
6	Pulsatile	up	50
7	Pulsatile	bottom	20
8	Pulsatile	bottom	50

The final computational grid employed a tetrahedral mesh, resulting in an average element size of approximately 100 mm, which was sufficient to resolve the velocity and temperature gradients around flow-control features.

Similar to a mesh independence study, the time-step size for the transient simulations was carefully selected. Multiple simulations with progressively smaller time-steps were performed, and the mass flow rate at the exhaust outlets was used as the primary convergence criterion. The time-step (120 s) was considered sufficiently small when the variation in outlet mass flow between two consecutively refined time-steps fell below 2%. This procedure ensures that the temporal discretization is fine enough to capture the dynamics of pulsatile ventilation. The final time-step value was therefore chosen to balance numerical accuracy with computational efficiency.

2.4 Evaluated Parameters

To assess the thermos-luid performance of the data center under various ventilation configurations, several flow and thermal quantities were extracted from the simulations for detailed analysis. The primary parameters included the air velocity field, used to identify jet behavior from the louvers and circulation patterns around the racks, and the temperature distribution, which enabled evaluation of heat removal efficiency and thermal stratification within the room. Streamlines were additionally generated to visualize global airflow organization and buoyancy-driven plumes above the heated racks.

For transient simulations with pulsatile inlet conditions, time-averaged temperatures were recorded at the monitoring points indicated in Figure 1 to quantify thermal fluctuations and long-term cooling performance. Furthermore, the mass flow rate at the outlet vents was evaluated at three key instances corresponding to the maximum, minimum, and mean inlet velocities, providing insight into the influence of velocity oscillations on ventilation effectiveness and extraction capacity. These parameters collectively form the basis for the comparative analysis presented in the Results section.

3 Result

The results presented in this study provide a comprehensive assessment of the airflow organization, thermal behavior, and ventilation effectiveness within the modeled data center under various inlet configurations. It is important to note that, for all transient simulations, the reported results correspond to the mean inlet velocity of 1.5 m/s unless otherwise specified. Only in cases where the discussion explicitly concerns the instantaneous flow state, such as the peak or minimum phases of the pulsatile cycle, are the results presented at their respective time-step velocities.

3.1 Control Temperature

Figure 2 illustrates the three-dimensional temperature distribution within the data center for the control configuration in which no ventilation inlets are active. In this geometric arrangement, the twelve heat-generating racks are the

only source of thermal energy, and air movement is governed solely by buoyancy forces induced by the temperature gradients inside the enclosure. Under these conditions, the maximum temperature (387°K) develops in the upper central region of the room, directly above the rack array, where rising thermal plumes accumulate due to the absence of forced convection. The minimum temperature (318°K) appears near the floor adjacent to the outer walls, where the air remains relatively undisturbed and retains its initial lower temperature. The temperature field exhibits a clear stratification pattern: strong vertical temperature gradients form above each rack ($>375^{\circ}\text{K}$), and these individual plumes merge into a wide, coherent hot layer beneath the ceiling. Across the domain, the contours reveal a monotonic upward increase in temperature up to 369°K , with limited horizontal spreading because no supply airflow exists to break or redistribute the rising buoyant jets. The control case demonstrates the worst thermal performance, highlighting the essential role of directed ventilation in maintaining acceptable temperature levels within the data center.

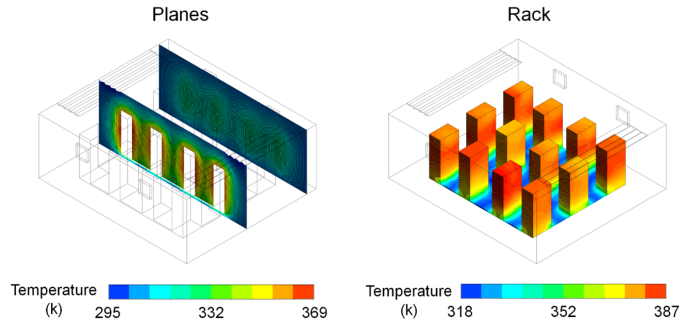


Figure 2. 3D temperature field showing severe heat buildup without ventilation

3.2 Air Velocity

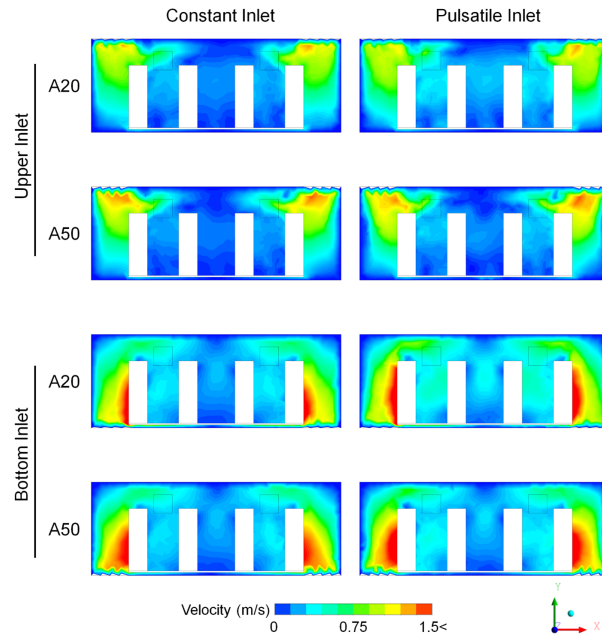


Figure 3. XY-plane velocity contours comparing airflow behavior across all ventilated cases

Figure 3 illustrates the airflow velocity contours in the horizontal (xy) plane for all eight ventilated configurations, combining the effects of inlet position (up or bottom), louver orientation (A20 or A50), and inlet velocity type (constant or pulsatile). In each configuration, the airflow enters through the designated louver and interacts with the rack array, producing distinct circulation zones and regions of accelerated or weakened flow. The geometric arrangement of the twelve racks creates narrow channels between rows, influencing how the inlet jet penetrates and redistributes air across the data center. In the A20 cases, the inlet jet remains closer to the horizontal direction, producing relatively longer but weaker flow penetration paths across the room. Consequently, the velocities reaching

to more than 1.5 m/s (maximum value) are consistently observed near the louver openings, where the incoming jet initially accelerates, whereas zero velocities appear in the shadow zones behind the central racks, where obstructions reduce momentum transfer. The flow structure shows smoother transitions and gradual decay of velocity magnitude as the jet interacts with the rack geometry. In contrast, the A50 configurations generate a steeper downward or upward jet trajectory (depending on inlet height), leading to more localized high-velocity regions near the racks directly in the jet path. The peak velocities shift (more than 1.2 m/s) closer to the rack surfaces, indicating stronger impingement and enhanced mixing. The lowest velocities occur along the far-side regions of the room, where the jet influence diminishes more rapidly than in A20 due to the sharper injection angle. The effect of inlet height is also evident. When the louver is positioned at the upper side, the jet descends into the rack corridor, forming recirculation pockets near the lower aisles. Conversely, in the bottom-inlet cases, the jet rises through the rack rows, enhancing upward transport and modifying the distribution of slow-moving zones near the ceiling. Pulsatile inflow cases exhibit a similar spatial velocity pattern but with increased variability in jet strength, causing the contours to show broader intermediate-speed regions compared to constant inflow conditions.

3.3 Room Temperature

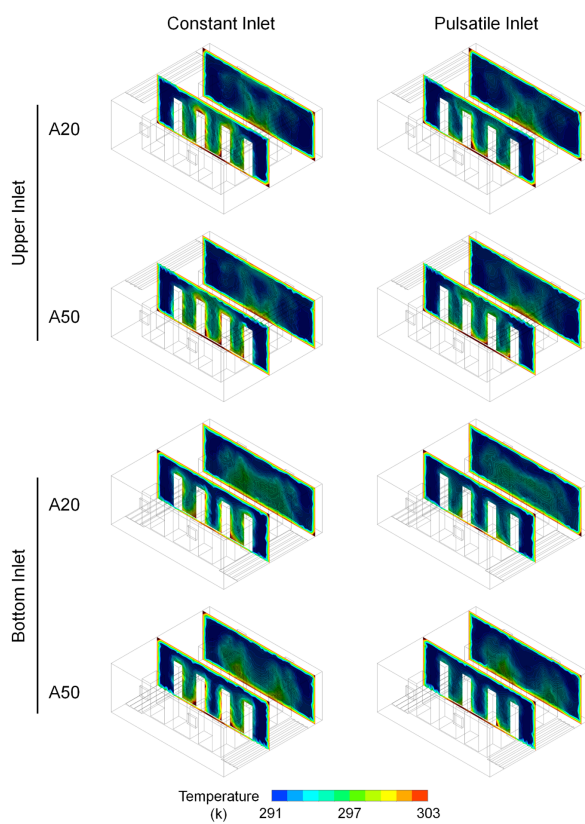


Figure 4. Temperature contours comparing cooling performance across all ventilated cases

Figure 4 illustrates the temperature contours in two horizontal (xy) planes for each of the eight ventilated configurations, with one plane positioned near the side wall and the other at the mid-plane of the data center. This dual-plane representation provides a clearer view of how inlet location (upper or bottom), louver angle (A20 or A50), and inlet velocity mode influence the spatial temperature distribution both near the enclosure boundaries and within the core region of the rack array. Across all cases, the temperatures of 303 °K appear in regions where buoyant hot air accumulates downstream of the rack rows, typically closer to the room center in the mid-plane slice and nearer the upper boundary along the wall-adjacent slice. The minimum temperatures occur near the louver entry zones, where the incoming 291 °K air first spreads into the domain. The near-wall plane captures sharper thermal gradients adjacent to the inlets (approximately 12 °K), while the mid-room plane highlights the development and interaction of plumes rising from the racks. In the A20 configurations, the shallower injection angle causes the inlet jet to sweep horizontally across both planes, producing more extended cool regions with temperature of 295 °K and smoother temperature transitions. Here, the cooling effect penetrates further into the domain, and the warmest zones tend to form toward the downstream end of the rack corridor. In contrast, the A50 configurations exhibit more localized cooling directly beneath the injection path, with steeper gradients and more confined low-temperature zones. The

higher angle produces quicker vertical deflection of the jet, leading to stronger plume-jet interactions in the mid-plane and more pronounced warm pockets near the far-wall section. Moreover, upper-inlet cases show a downward-directed cooling layer in the near-wall plane, while the mid-plane reveals delayed cooling penetration due to the jet striking the upper rack surfaces. Bottom-inlet cases, however, deliver cool air directly into the rack corridor, resulting in noticeably lower temperatures across the mid-plane and more uniform distribution near the wall plane. Although pulsatile and constant inlets share similar overall patterns, pulsatile cases display broader intermediate-temperature zones, reflecting the temporal variation in cooling strength.

3.4 Streamline

Figure 5 presents the temperature-colored streamlines for all eight ventilated configurations, highlighting how air introduced through different louver positions and orientations organizes the internal flow field and forms distinct circulation zones within the data center. In each panel, the streamlines emerge from the inlet louvers and traverse the rack aisles, allowing simultaneous interpretation of airflow trajectory and the associated temperature carried by each pathline. The overall pattern reveals that the main circulation loop consistently develops downstream of the racks, where rising buoyant flows encounter the upper boundary and are redirected toward the lateral walls. In addition, smaller vortical structures form between the racks, particularly in regions partially sheltered from the direct influence of the inlet jet, giving rise to pockets of reduced mixing where warmer air ($\sim 302 \text{ }^{\circ}\text{K}$) can become trapped. In the A20 configurations, the moderate injection angle guides the supply air horizontally for a longer distance before it bends upward. This produces broader, more coherent flow paths that sweep across a large portion of the central corridor. Under these conditions, recirculation zones tend to be weaker and more diffused, indicating a better distribution of momentum across the rack array. Temperature variations, from $292 \text{ }^{\circ}\text{K}$ to $303 \text{ }^{\circ}\text{K}$, along the streamlines remain relatively gradual, with warming occurring mainly as the flow is lifted into the upper layers of the room. The A50 configurations, however, exhibit a noticeably different behavior. The steeper louver orientation drives the inlet jet downward or upward more sharply depending on the inlet height, resulting in a more forceful interaction with the rack surfaces. This promotes the formation of compact, higher-intensity recirculation cells, particularly near the mid-rack elevation, and causes streamlines to undergo abrupt directional changes. Consequently, regions of confined circulation develop where warmer air persists for longer durations, as reflected by the elevated temperatures visible along these more tightly curved trajectories.

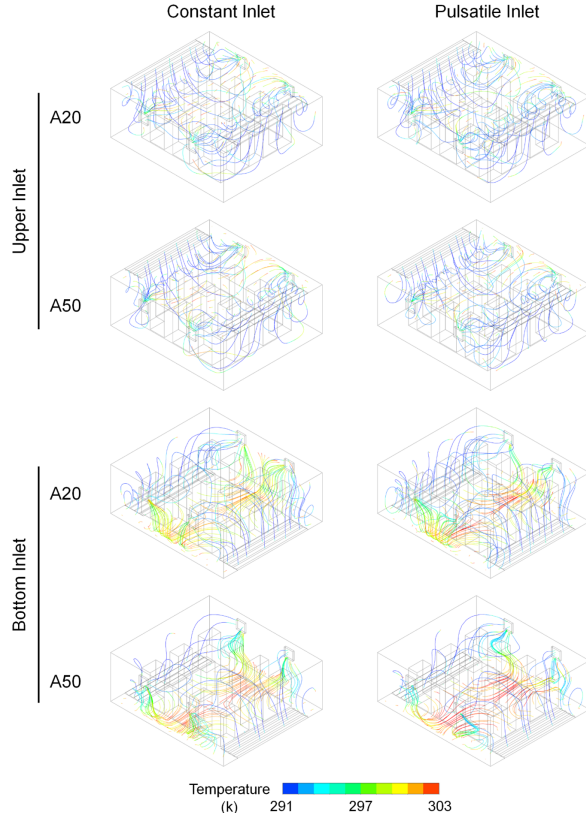


Figure 5. Temperature-colored streamlines showing airflow patterns across all ventilated cases

3.5 Rack Temperature

Figure 6 illustrates the temperature distribution on the rack surfaces, with the range of 321 °K to 366 °K, for all pulsatile ventilation configurations, with the left-hand panels representing the moment of maximum inlet velocity (1.9 m/s) and the right-hand panels corresponding to the minimum inlet velocity (1.1 m/s). Across all panels, a consistent pattern emerges: rack temperatures are noticeably lower during the high-velocity phase beginning with 321 °K, where the stronger jet enhances cooling penetration into the rack corridors and disrupts buoyant accumulation above the heated surfaces. Conversely, during the low-velocity phase, higher temperatures develop, particularly in the upper sections of the racks where thermal plumes recover strength as the inlet momentum weakens. Upper-inlet pulsatile cases show greater temperature reduction on the top portions of the racks during peak inflow, while bottom-inlet cases more effectively cool the lower and mid-level sections. When the velocity decreases, both configurations exhibit partial loss of cooling coverage, but the increase in temperature is more pronounced in regions farther from the louver jet.

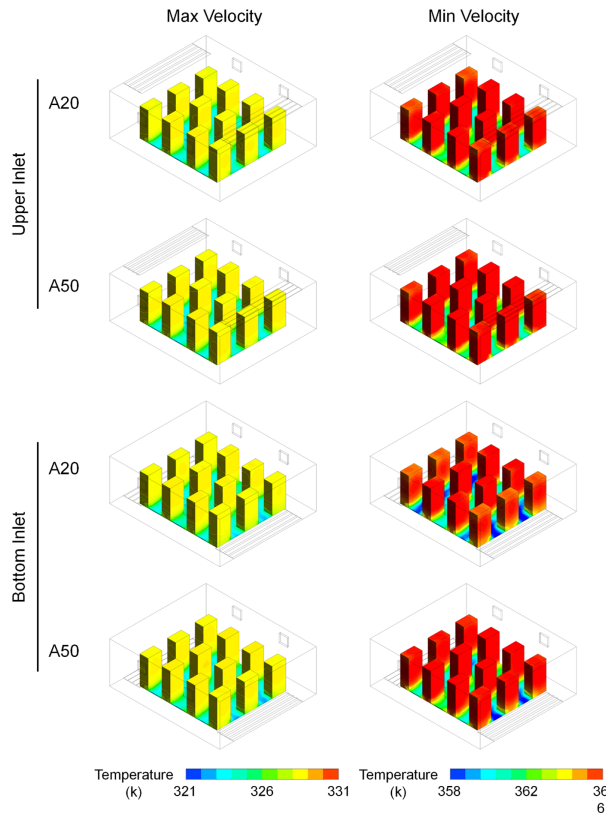


Figure 6. Rack surface temperatures comparing peak and minimum inlet velocities in pulsatile cases

3.6 Outlet Mass Flow

Figure 7 illustrates the mass-flow contours at the outlets for three phases of the pulsatile inlet condition: the minimum inlet velocity (1.1 m/s), the average velocity (1.5 m/s), and the maximum inlet velocity (1.9 m/s). In each panel, the mass-flow distribution across the outlet cross-section reveals how the instantaneous strength of the inlet jet governs extraction capacity within the data center. Under the minimum inlet velocity, the outlet exhibits the weakest mass-flow magnitude, with predominantly low negative values distributed symmetrically across the outlet area. The contours show limited momentum depletion near the vent center, indicating that buoyancy-driven upward motion, rather than forced ventilation, plays the dominant role during this phase. At the average inlet velocity, the mass-flow pattern becomes noticeably more uniform and more intense, with the mid-range contour band extending across a wider portion of the outlet surface. The increased extraction rate reflects the stronger supply jet, which enhances through-room circulation and facilitates more consistent removal of warmed air from the rack corridor. During the maximum inlet velocity, the outlet mass flow attains its highest magnitude, with deep blue regions indicating the most substantial negative mass-flow values. The contour field is more saturated and spatially expanded, demonstrating that the stronger jet significantly increases the exhaust capacity. The enhanced flow rate at this phase corresponds to the highest level of air exchange in the system, consistent with the expected peak of the pulsatile ventilation cycle.

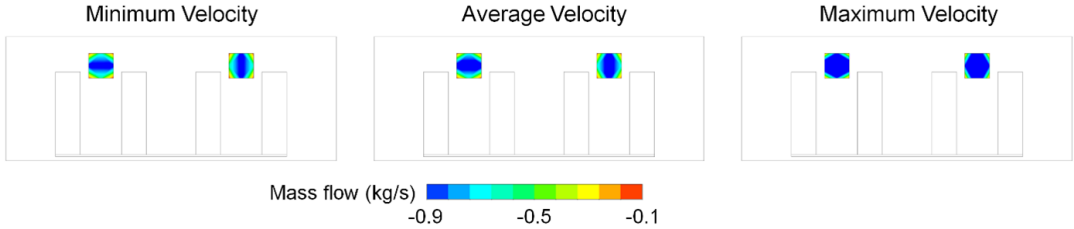


Figure 7. Outlet mass-flow contours showing exhaust variation across pulsatile phases

3.7 Time-Averaged Temperature

Figure 8 illustrates the time-averaged temperature profiles at the seven monitoring points defined in Figure 1 for the pulsatile inlet simulations, with the left panels corresponding to the upper-louver configurations and the right panels representing the bottom-louver configurations. Each curve tracks the evolution of the mean temperature over the full one-hour simulation period, allowing assessment of long-term thermal behavior under oscillating inlet conditions. In the upper-inlet cases, the cooling effect reaches the upper monitoring points more rapidly, resulting in comparatively lower mean temperatures in regions near the ceiling and the upper sections of the rack corridor. Points located deeper within the room, particularly those positioned downstream of the rack array, show a gradual increase in mean temperature due to the persistence of buoyant plumes that are only partially counteracted by the descending inlet jet. The temperature curves for these points exhibit moderate fluctuations early in the simulation before stabilizing toward the end of the hour. In contrast, the bottom-inlet configurations demonstrate improved cooling at the lower and mid-level points, where the upward-directed jet interacts directly with the rising hot air from the racks. As a result, these points maintain lower time-averaged temperatures compared to their counterparts in the upper-inlet cases. However, monitoring points located closer to the ceiling experience higher mean temperatures, as the upward-moving jet delivers limited cooling to the upper domain during the weaker phases of the pulsatile cycle.

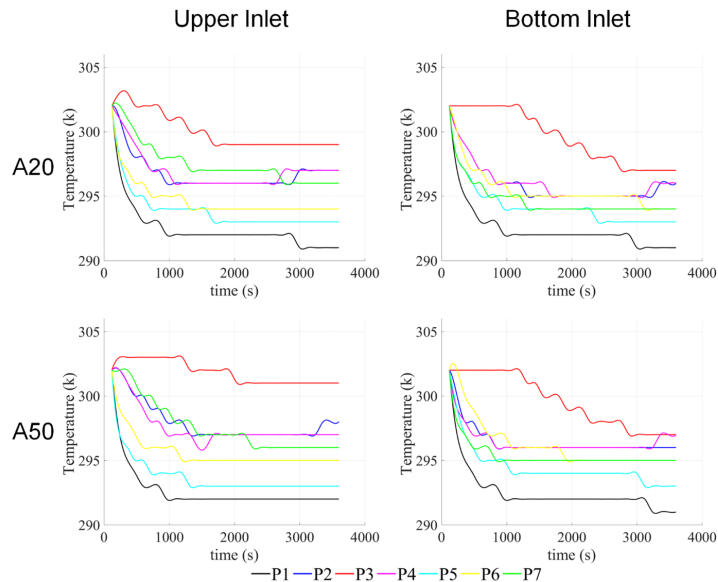


Figure 8. Time-averaged temperatures showing the effect of inlet height on thermal distribution

4 Discussion

The temperature distribution observed in the control configuration reveals several fundamental thermal behaviors characteristic of enclosed data center environments lacking directed ventilation. The strong thermal stratification and plume accumulation over the rack array indicate that buoyancy alone is insufficient for removing heat generated by densely arranged equipment. This behavior aligns with earlier studies demonstrating that natural convection in confined server rooms leads to vertical temperature layering and inadequate extraction of waste heat, particularly near the upper region of the enclosure [34, 35]. However, the magnitude and spatial extent of the hot layer in the present

configuration appear more pronounced than in some previous CFD studies of passive cooling in data centers [36]. This geometric constraint therefore intensifies stratification compared with taller, more open architectures.

The airflow behavior observed in Figure 3 demonstrates how inlet height, louver orientation, and inlet velocity mode jointly shape momentum distribution across the data center. The formation of high-velocity jets near the louver openings and the development of low-momentum zones behind the central racks are strongly governed by geometric obstruction and the angle at which supply air is injected. The smoother velocity transitions observed in the A20 configurations align with earlier findings in angled-inlet ventilation systems, where shallower injection angles were shown to enhance lateral coverage and reduce local stagnation [7]. In this regard, the present results support the expectation that a lower louver angle promotes broader momentum dispersion before buoyancy effects redirect the flow upward. However, the sharper jet trajectories seen in the A50 configurations differ from some studies where steep injection angles produced a more uniform spread across rack aisles, particularly when ceiling height was larger and jet entrainment could develop more effectively [23]. In the current geometry, the relatively limited vertical clearance and dense rack arrangement restrict entrainment, causing the air stream to remain confined along a narrow path and resulting in localized high-velocity regions near the jet's immediate impact zone. This explains why the present results show stronger impingement and steeper momentum decay for A50 compared with earlier studies conducted in more open environments.

The differences between upper- and bottom-inlet configurations are also consistent with general principles of mixed convection. Bottom inlets naturally reinforce buoyancy-driven upward motion, producing clearer vertical pathways, whereas upper inlets oppose buoyant rise and therefore generate more complex recirculation patterns in the lower aisles. Similar behaviors were reported in data center ventilation studies examining ceiling-based cooling systems, where descending cold jets produced counter-rotating vortices near the floor [37]. The present results show a comparable pattern, indicating that the interaction between jet momentum and buoyant plumes is a dominant mechanism shaping the flow field.

Pulsatile inlet cases exhibit broader intermediate-velocity regions, suggesting enhanced temporal mixing; however, the fundamental spatial distribution remains dictated by geometry and louver orientation. This observation agrees with studies showing that unsteady inflow modulates local mixing without drastically modifying overall flow topology in confined domains [38]. The slight deviations between the present findings and those of studies that report stronger pulsation-driven restructuring of recirculation zones may be attributed to differences in pulsation amplitude, inlet area, and room scale.

The temperature contours presented in Figure 4 highlight how variations in inlet placement and louver angle shape the thermal field both near the boundaries and within the rack corridor. The contrast between the near-wall and mid-plane slices emphasizes the role of jet momentum, jet direction, and buoyancy interaction in determining the spread of cool air across the data center. The observed temperature layering and the formation of downstream warm regions align with established findings that buoyancy-driven accumulation is amplified when forced convection does not penetrate deeply into the central equipment zone [39]. The broader cooling footprint observed in A20 configurations is consistent with earlier work demonstrating that shallow-angle supply flows enhance horizontal coverage and delay vertical temperature rise by suppressing plume coalescence [40]. In these studies, reduced jet inclination allowed the supply stream to travel farther before lifting, which closely resembles the extended cool zones seen in the present A20 cases. Conversely, the more confined cooling patterns and sharper gradients in A50 configurations correspond with prior reports showing that steep supply angles promote early jet lifting and stronger interaction with rising plumes, often resulting in localized cooling accompanied by persistent warm regions downstream [41]. The broader intermediate-temperature zones in pulsatile cases align with research demonstrating that unsteady inflow can enhance local mixing without substantially altering overall stratification patterns [37]. These works indicate that pulsation weakens temperature gradients but does not fully disrupt plume-driven layering when geometry remains the dominant constraint, consistent with the trends observed in Figure 4.

Streamline analysis confirms that louver angle and inlet height dictate recirculation zones. Shallower angles (A20) enhance lateral jet penetration, weakening vortices, while steeper angles (A50) intensify jet-plume interaction and localized recirculation [40]. Bottom inlets reinforce buoyant upward flow [36], whereas upper inlets promote lower-aisle counter-rotating vortices [42, 43]. Critically, strong recirculation cells trap warmer air, indicating prolonged residence time and poor mixing.

Rack surface temperatures during pulsatile ventilation demonstrate the strong coupling between inlet momentum and buoyancy recovery. Peak inlet velocity reduces temperatures by enhancing jet penetration and suppressing thermal plumes [44]. Conversely, minimum velocity causes elevated upper-rack temperatures, mirroring buoyancy-driven rebound. Discrepancies with studies reporting uniformity likely stem from larger aisle geometries. The influence of inlet height is also consistent: top inlets effectively cool upper thermal layers, while bottom inlets preferentially cool the rack base.

The mass-flow variations across the pulsatile cycle reflect the direct modulation of extraction capacity by inlet momentum. The increase in outlet mass flow at higher inlet velocities agrees with prior work showing that transient

high-momentum supply enhances exhaust efficiency and suppresses buoyancy dominance [45, 46].

Time-averaged temperatures show that inlet height governs the long-term balance between forced momentum and buoyancy. Top-louver configurations induce faster cooling at upper points by breaking up ceiling-level stratification and suppressing plumes [36, 47]. Conversely, bottom-inlet cases achieve sustained temperature reduction at lower/mid-levels by intercepting rising plumes effectively [48]. The gradual downstream warming aligns with partial buoyancy recovery between momentum peaks in transient study [48]. Discrepancies with reports of uniform top-zone cooling are likely due to geometric differences, such as restricted upper free volume in the current enclosure.

The inclusion of pulsatile (time-varying) inlet airflow alongside a baseline steady inflow was motivated by both thermal management and energy-efficiency considerations. While the constant-flow inlet ensures a reliable baseline cooling, the superimposed pulsatile component allows the airflow to adapt dynamically to local and transient thermal loads within the data center. The thermal mass of the air and server racks provides short-term buffering, which enables periodic modulation of the cooling flow without exceeding recommended rack inlet temperatures. This strategy reduces the overall energy consumption of the cooling system, as fan power scales approximately with the cube of the airflow rate. Additionally, the pulsatile inflow enhances mixing in the cold aisle and mitigates localized hot spots by periodically redistributing air across the enclosure. As a result, the combination of steady and pulsatile ventilation improves both the temperature uniformity and energy efficiency of the data center, offering a more realistic representation of modern demand-modulated cooling strategies compared to purely steady-state simulations.

5 Conclusion

This study investigated the thermos-fluid behavior inside a medium-sized data center equipped with twelve heat-generating racks under various ventilation strategies involving different inlet positions, louver orientations, and inflow conditions. The results highlight the dominant role of airflow organization, more than merely the presence of ventilation, in determining cooling effectiveness, thermal uniformity, and the formation of recirculation zones.

Across all configurations, the comparison with the unventilated control case confirms that directed ventilation is essential for suppressing thermal stratification and preventing the accumulation of persistent hot layers above the racks. Among the ventilated scenarios, the louver angle and inlet height emerged as critical design parameters. Shallower-angle louvers (A20) produced longer horizontal penetration and weaker recirculation pockets, leading to more uniform cooling across the rack corridor. In contrast, steeper louvers (A50) intensified localized recirculation, generating confined high-temperature pockets that reduced thermal performance.

The inlet position strongly influenced vertical temperature distribution. Bottom-inlet configurations effectively cooled the lower and mid-rack regions by intercepting buoyant plumes close to their origin, whereas top-inlet configurations were more successful in disrupting the upper hot layer and reducing ceiling-level stratification. These complementary behaviors underscore the importance of selecting inlet height according to the dominant cooling objectives and internal layout constraints.

The pulsatile ventilation cases demonstrated notable advantages over constant inflow. Periodic high-momentum phases improved mixing, strengthened cold-air penetration, and temporarily suppressed buoyancy, resulting in lower rack temperatures and broader regions of intermediate cooling. However, during low-momentum phases, buoyancy partially recovered, which highlights the dynamic balance between forced and natural convection in data centers with transient ventilation strategies.

Finally, mass-flow analysis revealed that extraction capacity at the outlet vents is highly sensitive to fluctuations in inlet momentum, especially in geometrically confined environments. The strongest outlet flows occurred during the peak of the pulsatile cycle, indicating that dynamic ventilation enhances through-room air exchange more effectively than steady operation.

In practical engineering terms, the results of this study suggest that shallow-angle louvers combined with strategically placed inlets, particularly configurations that leverage pulsatile inflow, represent the most promising ventilation architecture for real-world data-center deployment. These configurations simultaneously enhance cold-air penetration, suppress recirculation zones, and improve thermal uniformity, making them suitable for medium-sized facilities with high rack density. Looking forward, several avenues can further refine the applicability of these findings. Full-scale on-site evaluations under variable server loads and seasonal boundary conditions would help assess operational robustness. Integrating control-oriented simulations, where inlet pulsing frequency and amplitude adapt to real-time thermal feedback, may unlock additional energy savings. Moreover, coupling the ventilation strategy with predictive cooling management such as AI-based hotspot forecasting or workload-aware thermal routing, could transform these design recommendations into an active thermal-optimization framework. Such advancements will help bridge the gap between computational insights and deployable engineering solutions for next-generation, energy-efficient data-center environments.

Overall, the findings emphasize that optimizing data-center ventilation requires simultaneous consideration of inlet geometry, placement, and temporal forcing. The combination of a shallow louver angle, strategically selected inlet height, and pulsatile operation offers a promising pathway for improving cooling performance while reducing thermal

non-uniformities. These insights can inform the design of more energy-efficient and thermally stable data-center environments.

Author Contributions

Conceptualization, L.R. and A.N.; methodology, A.N. and M.M.; software, L.R. and A.N.; validation, A.N. and M.M.; formal analysis, A.N.; data curation, L.R.; writing—original draft preparation, A.N. and M.M.; writing—review and editing, A.N. and M.M.; visualization, L.R. All authors have read and agreed to the published version of the manuscript.

Data Availability

The data used to support the research findings are available from the corresponding author upon request.

Conflicts of Interest

The authors declare no conflict of interest.

References

- [1] S. Ilager and R. Buyya, “Energy and thermal-aware resource management of cloud data centres: A taxonomy and future directions,” *arXiv*, p. arXiv:2107.02342, 2021. <https://doi.org/10.48550/arXiv.2107.02342>
- [2] S. Cai and Z. Gou, “Towards energy-efficient data centers: A comprehensive review of passive and active cooling strategies,” *Energy Built Environ.*, 2024. <https://doi.org/10.1016/j.enbehv.2024.08.009>
- [3] X. Gao, G. Liu, Z. Xu, H. Wang, L. Li, and X. Wang, “Investigating security vulnerabilities in a hot data center with reduced cooling redundancy,” *IEEE Trans. Dependable Secure Comput.*, vol. 19, no. 1, pp. 208–226, 2020. <https://doi.org/10.1109/TDSC.2020.2977292>
- [4] X. Zhang, T. Lindberg, N. Xiong, V. Vyatkin, and A. Mousavi, “Cooling energy consumption investigation of data center IT room with vertical placed server,” *Energy Procedia*, vol. 105, pp. 2047–2052, 2017. <https://doi.org/10.1016/j.egypro.2017.03.581>
- [5] A. Safari, H. Sorouri, A. Rahimi, and A. Oshnoei, “A systematic review of energy efficiency metrics for optimizing cloud data center operations and management,” *Electronics*, vol. 14, no. 11, p. 2214, 2025. <https://doi.org/10.3390/electronics14112214>
- [6] E. Vibron, A. L. Ljung, and T. S. Lundström, “Computational fluid dynamics modeling and validating experiments of airflow in a data center,” *Energies*, vol. 11, no. 3, p. 644, 2018. <https://doi.org/10.3390/en11030644>
- [7] S. A. Nada, M. A. Said, and M. A. Rady, “CFD investigations of data centers’ thermal performance for different configurations of CRACs units and aisles separation,” *Alexandria Eng. J.*, vol. 55, no. 2, pp. 959–971, 2016. <https://doi.org/10.1016/j.aej.2016.02.025>
- [8] N. M. S. Hassan, M. M. K. Khan, and M. G. Rasul, “Temperature monitoring and CFD analysis of data centre,” *Procedia Eng.*, vol. 56, pp. 551–559, 2013. <https://doi.org/10.1016/j.proeng.2013.03.159>
- [9] K. Mohammed Faisal and M. Jeoju, “Analysis and performance prediction of data centre with different configurations using CFD,” *Int. J. Eng. Res. Technol.*, vol. 4, no. 10, pp. 570–575, 2015.
- [10] S. Gilani, H. Montazeri, and B. Blocken, “CFD simulation of stratified indoor environment in displacement ventilation: Validation and sensitivity analysis,” *Build. Environ.*, vol. 95, pp. 299–313, 2016. <https://doi.org/10.1016/j.buildenv.2015.09.010>
- [11] T. Gao, B. Sammakia, E. Samadiani, and R. Schmidt, “Steady state and transient experimentally validated analysis of hybrid data centers,” *J. Electron. Packag.*, vol. 137, no. 2, p. 021007, 2015. <https://doi.org/10.1115/1.4029163>
- [12] R. K. Sharma, C. E. Bash, C. D. Patel, R. J. Friedrich, and J. S. Chase, “Balance of power: Dynamic thermal management for Internet data centers,” *IEEE Internet Comput.*, vol. 9, no. 1, pp. 42–49, 2005. <https://doi.org/10.1109/MIC.2005.10>
- [13] J. Cho, B. Park, and Y. Jeong, “Thermal performance evaluation of a data center cooling system under fault conditions,” *Energies*, vol. 12, no. 15, p. 2996, 2019. <https://doi.org/10.3390/en12152996>
- [14] J. Zhang and Y. Jaluria, “Steady and transient behavior of data centers with variations in thermal load and environmental conditions,” *Int. J. Heat Mass Transf.*, vol. 108, pp. 374–385, 2017. <https://doi.org/10.1016/j.ijheatmasstransfer.2016.12.028>
- [15] S. K. Shrivastava and M. Ibrahim, “Benefit of cold aisle containment during cooling failure,” in *International Electronic Packaging Technical Conference and Exhibition*, vol. 55768, California, USA, 2013, p. V002T09A021. <https://doi.org/10.1115/IPACK2013-73219>
- [16] N. Lazic, T. Lu, C. Boutilier, M. Ryu, E. Wong, B. Roy, and G. Imwalle, “Data center cooling using model-predictive control,” in *Proceedings of the 32nd International Conference on Neural Information Processing Systems*, Montréal, Canada, 2018, pp. 1–10.

- [17] A. Heimerson, J. Sjölund, R. Brännvall, J. Gustafsson, and J. Eker, “Adaptive control of data center cooling using deep reinforcement learning,” in *2022 IEEE International Conference on Autonomic Computing and Self-Organizing Systems Companion (ACSOS-C)*, CA, USA, 2022, pp. 1–6. <https://doi.org/10.1109/ACSOSC56246.2022.00018>
- [18] G. Hu, Z. Wang, Y. Fan, H. Yuan, and Q. Gao, “Study on the disturbance effect of pulsating flow and heat transfer in self-excited oscillation shear layer,” *Therm. Sci.*, vol. 26, no. 4, pp. 3157–3170, 2022. <https://doi.org/10.2298/TSCI210611347H>
- [19] S. Irving, “The role of ventilation in cooling non-domestic buildings,” 1996.
- [20] V. Avelar, “How overhead cabling saves energy in data centers,” APC by Schneider Electric, White Paper 159, 2011. https://www.facilitiesnet.com/whitepapers/pdfs/APC_102412.pdf
- [21] L. Silva-Llanca, M. Del Valle, A. Ortega, and A. J. Díaz, “Cooling effectiveness of a data center room under overhead airflow via entropy generation assessment in transient scenarios,” *Entropy*, vol. 21, no. 1, p. 98, 2019. <https://doi.org/10.3390/e21010098>
- [22] H. Kokash, “Optimization through CFD analysis of a Coanda effect enhanced novel HVAC diffuser,” Master’s thesis, University of Michigan-Flint, 2020.
- [23] A. Awwad, M. H. Mohamed, and M. Fatouh, “Study the effect of ceiling air diffuser blade and lip angles using CFD,” *Athens J. Technol. Eng.*, vol. 4, no. 4, pp. 309–358, 2017.
- [24] H. Kokash, M. G. Burzo, K. Khanafer, and B. Gokeda, “Investigation of a Coanda-effect enhanced HVAC diffuser using CFD analysis,” in *Proceedings of the ASME 2021 International Mechanical Engineering Congress and Exposition (IMECE2021)*, 2021. <https://doi.org/10.1115/IMECE2021-69036>
- [25] M. Lappa, “Incompressible flows and the Boussinesq approximation: 50 years of CFD,” *C. R. Mec.*, vol. 350, no. S1, pp. 75–96, 2022. <https://doi.org/10.5802/crmeca.134>
- [26] J. Liu, S. Zhu, M. K. Kim, and J. Srebric, “A review of CFD analysis methods for personalized ventilation (PV) in indoor built environments,” *Sustainability*, vol. 11, no. 15, p. 4166, 2019. <https://doi.org/10.3390/su11154166>
- [27] M. M. Othayq, “CFD investigation on the thermal comfort for an office room,” *Buildings*, vol. 15, no. 15, p. 2802, 2025. <https://doi.org/10.3390/buildings15152802>
- [28] D. Macedo, R. Godina, P. Dinis Gaspar, P. D. da Silva, and M. Trigueiros Covas, “A parametric numerical study of the airflow and thermal performance in a real data center for improving sustainability,” *Appl. Sci.*, vol. 9, no. 18, p. 3850, 2019. <https://doi.org/10.3390/app9183850>
- [29] X. Huang, J. Yan, X. Zhou, Y. Wu, and S. Hu, “Cooling technologies for Internet data center in China: Principle, energy efficiency, and applications,” *Energies*, vol. 16, no. 20, p. 7158, 2023. <https://doi.org/10.3390/en16207158>
- [30] N. Gao, S. M. Ali, and T. Persoons, “On the numerical investigation of two-phase evaporative spray cooling technology for data centre applications,” *Fluids*, vol. 9, no. 12, p. 284, 2024. <https://doi.org/10.3390/fluids9120284>
- [31] M. K. Patterson, “The effect of data center temperature on energy efficiency,” in *2008 11th Intersociety Conference on Thermal and Thermomechanical Phenomena in Electronic Systems*, Orlando, FL, USA, 2008, pp. 1167–1174. <https://doi.org/10.1109/ITHERM.2008.4544393>
- [32] A. M. Almoli, “Air flow management inside data centres,” Ph.D. dissertation, University of Leeds, 2013.
- [33] A. Dogan, S. Yilmaz, M. Kuzay, C. Yilmaz, and E. Demirel, “CFD modeling of pressure drop through an OCP server for data center applications,” *Energies*, vol. 15, no. 17, p. 6438, 2022. <https://doi.org/10.3390/en15176438>
- [34] L. W. Chew and N. X. R. Tan, “Thermal stratification in a full-scale room under buoyancy-driven displacement ventilation,” in *Proceedings of the Healthy Buildings Asia*, Tianjin, China, 2023.
- [35] K. Khanafer and K. Vafai, “Buoyancy-driven flow and heat transfer in open-ended enclosures: Elimination of the extended boundaries,” *Int. J. Heat Mass Transf.*, vol. 43, no. 22, pp. 4087–4100, 2000. [https://doi.org/10.1016/S0017-9310\(00\)00047-8](https://doi.org/10.1016/S0017-9310(00)00047-8)
- [36] E. Wibron, “CFD modeling of an air-cooled data center,” Master’s thesis, Chalmers University of Technology, 2015.
- [37] B. E. Falleni, A. Sattari, J. H. Fransson, and M. Sandberg, “Experimental study on the effect of pulsating inflow to an enclosure for improved mixing,” *Int. J. Heat Fluid Flow*, vol. 44, pp. 108–119, 2013. <https://doi.org/10.1016/j.ijheatfluidflow.2013.05.004>
- [38] E. Mesenhöller, P. Vennemann, and J. Hussong, “Unsteady room ventilation—A review,” *Build. Environ.*, vol. 169, p. 106595, 2020. <https://doi.org/10.1016/j.buildenv.2019.106595>
- [39] E. N. El-Sayed, I. A. Stefanovici, G. Amvrosiadis, A. A. Hwang, and B. Schroeder, “Temperature management in data centers: Why some (might) like it hot,” in *Proceedings of the 12th ACM SIGMETRICS/PERFORMANCE Joint International Conference on Measurement and Modeling of Computer Systems*, London, United Kingdom, 2012, pp. 163–174. <https://doi.org/10.1145/2254756.2254778>
- [40] S. R. Traboulisi, A. Hammoud, and M. F. Khalil, “Effects of jet inclination angle and geometrical parameters on

- air curtain performance,” *ASHRAE Trans.*, vol. 115, no. 2, pp. 617–624, 2009.
- [41] R. Gao, M. Liu, Q. Zheng, Z. Zhang, R. Jing, A. Li, W. Lei, and L. Zhang, “High-efficiency diffuser based on a normalized evaluation index of jet length and resistance,” *Build. Environ.*, vol. 195, p. 107737, 2021. <https://doi.org/10.1016/j.buildenv.2021.107737>
- [42] T. van Hooff, B. Blocken, and Y. Tominaga, “On the accuracy of CFD simulations of cross-ventilation flows for a generic isolated building: Comparison of RANS , LES and experiments,” *Build. Environ.*, vol. 114, pp. 148–165, 2017. <https://doi.org/10.1016/j.buildenv.2016.12.019>
- [43] M. Zhang, Z. Zhang, Y. Hu, Y. Geng, H. Huang, and Y. Huang, “Effect of raised floor height on different arrangement of under-floor air distribution performance in data center,” *Procedia Eng.*, vol. 205, pp. 556–564, 2017. <https://doi.org/10.1016/j.proeng.2017.10.425>
- [44] C. Dang, L. Jia, and Q. Lu, “Investigation on thermal design of a rack with the pulsating heat pipe for cooling CPUs,” *Appl. Therm. Eng.*, vol. 110, pp. 390–398, 2017. <https://doi.org/10.1016/j.applthermaleng.2016.08.187>
- [45] P. Mayeli and G. J. Sheard, “Buoyancy-driven flows beyond the Boussinesq approximation: A brief review,” *Int. Commun. Heat Mass Transf.*, vol. 125, p. 105316, 2021. <https://doi.org/10.1016/j.icheatmasstransfer.2021.105316>
- [46] K. Wu, J. Xiao, and L. M. Ni, “Rethinking the architecture design of data center networks,” *Front. Comput. Sci.*, vol. 6, no. 5, pp. 596–603, 2012. <https://doi.org/10.1007/s11704-012-1155-6>
- [47] V. Tuninetti, B. Ales, and T. Mora Chandía, “Numerical and experimental analysis of thermal stratification in locally heated residential spaces,” *Buildings*, vol. 15, no. 14, p. 2417, 2025. <https://doi.org/10.3390/buildings15142417>
- [48] L. Puggioni, G. Boga, A. Cimarelli, M. C. Esposito, S. Musacchio, E. Stalio, and G. Boffetta, “Transition to the buoyancy-dominated regime in a planar temporal forced plume,” *J. Fluid Mech.*, vol. 1002, p. A43, 2025. <https://doi.org/10.1017/jfm.2024.1237>